Experimentelle und numerische Untersuchungen eines Tiefseewasser-Simulator bei Druckauf-und Druckabbau

Experimental and numerical studies during pressurization and depressurization phases inside a Deep Sea Simulator

J.Y. Ko[1,2], J.R. Agudo[1], J. Park[1], G. Luzi[1], C. Rauh[1,2,3], A. Wierschem[2], A. Delgado[1,2]

[1]Institute of Fluid Mechanics, FAU Busan Campus, University of Erlangen-Nuremberg, 618-230 Busan, Republic of Korea
[2]Institute of Fluid Mechanics, University of Erlangen-Nuremberg, D-91058 Erlangen, Germany
[3]Department of Food Biotechnology and Food Process Engineering Technische Universität Berlin
D-14195 Berlin, Germany

Methanhydrat, Umwelttechnik, Energietechnik.
Methane Hydrate, Green technology, Energy technology.

Abstract

During the last decade, Gas Hydrate (GH) formation-dissociation processes have attracted the interest of the scientific community. Methane Hydrate (MH), for instance, is considered as one of the most important potential source for hydrocarbon fuel. Carbon dioxide hydrate (CO_2H), on the other hand, may be of vital importance for capture and sequestration methods in order to reduce global climate change. The transport phenomena involved on the physical-chemical processes taking place during GH formation-dissociation under submarine conditions are not yet fully understood. An exhaustive study is required to ensure a safe and ecological manipulation of GH. For that purpose, we have installed at the university campus of FAU Busan (Korea) a high pressure vessel (Deep Sea Simulator) which mimics the submarine conditions of GH deep oceanic deposits. In order to characterize the Simulator, first, an extensive set of PIV measurements on two different planes following the effect of pressurization and depressurization phases has been conducted. Besides, numerical simulations have been performed and compared to the experimental results. In a good agreement with experiments, numerics reveal recirculation currents which take place inside the vessel and remain several minutes after pressurization stopped. The good concordance demonstrates the applicability of PIV measurement technique to flows under high pressure. Finally, PIV measurements are performed to qualitative study the onset of GH dissociation. The flow velocity generated as a consequence of the gas relief into the bulk of water can be characterized as a function of the deviation degree from gas hydrate stability conditions (GHSC).

Introduction

Natural gas hydrates are crystalline solids composed of water and gas. The gas molecules are trapped in water cavities that are composed of water molecules (Sloan, Koh, 2008). Typical natural gas molecules are methane, ethane, propane and carbon dioxide. In nature, this gas is usually methane. Methane gas is thermodynamically stabilized within the hydrate due to interactions of van der Waals forces between gas and crystalline lattice of water molecules held together by hydrogen bonds.

The estimated amount of organic carbon in the methane hydrate reservoir greatly exceeds that in many other reservoirs of the global carbon cycle. The energy density of methane hydrate is 2-5 times greater than the energy density of conventional natural gas (Kvenvolden, 1993). The combustion of methane produces less CO_2 than any other hydrocarbon. Therefore, methane hydrate (MH) is considered as an ideal alternate of energy resource and it may constitute a future source of natural gas.

Various research programs also actively focus on the ocean disposal of fossil fuel CO_2 as means for sequestering CO_2 to reduce climate impact (Bachu, 2000; Kajishima et al., 1997; Haugan, Drange, 1992). CO_2 injection into a methane hydrate reservoir can further enhance the production of natural gas from hydrate deposits (Janicki et al., 2014; McGrail et al., 2007). Therefore, methane recovery combined with capture and storage of CO_2 as CO_2H seem to be a promising technology.

The production of methane hydrates is fundamentally different from extraction of oil and natural gas. These conventional fuels flow naturally through the pores of the reservoirs to the well. Hydrates, on the other hand, must first be dissociated. Stability is thus a key aspect in modeling dissociation and dissolution in various geological settings (Zhang et al., 2012). Methane hydrate is very sensitive to its environment. Fluctuations in pressure, temperature, salinity, degree of gas saturation or sediment bed properties may cause methane gas release from the water lattice. Methane is a potent greenhouse gas and may therefore cause negative impact on climate changes. Also, GH dissociation may cause seafloor landslides. Latest research reveals the possible implication for the formation of tsunamis and continental slope failures (Kim et al., 2013). For all these reasons, several approaches had been established to determine the stability of methane hydrate. For example, stability of methane hydrate in seawater had been calculated based on empirical algorithms (Tishchenko et al., 2005).

For this purpose, we have designed a high pressure vessel (Deep Sea Simulator), which mimics the deep sea condition of methane hydrate deposits (Agudo et al., 2015). The vessel is able to achieve the maximum pressure of 150 bar, keeping the temperature of about 475 L of seawater constant at 3-4 °C. The design of this simulator includes 8 sapphire windows, which ensure optical accessibility. Thus, non-invasive optical methods such as Particle Image Velocimetry (PIV) can be used. Following experimental measurements, simulation models are developed to validate the results. Hence, disturbances and instabilities can be predicted in the future to ensure a safe extraction of methane hydrate. The main aim of the present research project is to study whether fluctuations in the environment, as for instance caused by changes in pressure, water temperature or velocity occur during pressurization and depressurization processes. They are crucial for the stability of methane hydrate (Archer, 2007)

Experimental Set-up

Experiments are conducted in a Deep Sea Simulator (see Fig. 1) with a total volume of 475 L connected to a cooling tank filled with water which is cooled up to 4°C. The cooled water is injected into the vessel. After the vessel is filled with water, pressurization and depressurization processes are carried out.

PIV measurements have been performed to characterize the flow velocity profile during pressurization and depressurization phases with water inside the deep sea simulator. It is carried out by using a 532 nm double pulse Nd: Yag laser to illuminate silver coated hollow glass tracers of 10 μm in diameter, as shown in Fig. 1 (a). Given the low flow velocity inside the pressure vessel, the time delay between laser pulses is chosen to be 60 ms. The light scattering by the tracer particles is detected and recorded with a 2 MP charge-couple device (CCD) camera coupled with a 50 mm lens. A programmable master timing control unit synchronizes camera and laser pulses. The design of the vessel offers 14 inlets or outlets for experimental instrumentation. The pressurization and depressurization processes are carried out at inlet and outlets of diameter 10 mm which are situated at different locations shown in Fig. 1. For our study purpose, pressurization is carried out by injection of water through the center inlet to increase the pressure to 100 bar. For the full elucidation of pressurization condition, the

instant flow velocity field is determined before pressurization to 30 minutes after pressurization until no more flow change is identified. For depressurization studies, the valve at the center or top outlet at the back side wall will be opened. By opening the valve, pressure is decreased to 10 bar.

The instantaneous flow velocities are taken at the observation areas on horizontal and vertical planes at a distance of 0.155 m from the center at the back side wall of the high pressure vessel with PIV. The horizontal plane as seen in Fig. 1 corresponds to a circular area with a diameter of 60 mm. We refer to (Agudo et al., 2015) for further details of the PIV experiments.

Numerical approach

The computational fluid dynamics (CFD) model of the Deep Sea Simulator has been developed with commercial software ANSYS CFX 15.0®. The geometry of the cylindrical reactor with a length of 1.8 m and a diameter of 0.58 m displayed in Fig. 1 is built with ANSYS ICEM 15.0®. The computational domain is endorsed by 4 sections: back and front side walls, the cylindrical wall and the inlet or outlet.

To obtain an accurate numerical computation, a grid convergence study is carried out. The spatial as well as temporal discretization accuracies are determined. For each pressurization and depressurization process, four grids are developed, respectively. A mesh refinement factor of 1.6 is chosen. Non-uniform hexahedral grid is used, and the mesh is refined near the walls where velocity gradients have to be accurately resolved. Additionally, grids at the observation areas are further refined accordingly.

In order to perform the grid independence study, the maximum values of velocities at the observation area are chosen. Besides we compute the Grid Convergence Index (GCI) to estimate how far is the solution from the asymptotic numerical value, and how much it would change if the grid is additionally refined. All meshes result in a ratio of GCI of about 1 which shows that the values of maximum velocity converge gradually to a limit, when mesh elements increases. Optimal grid and time step size are chosen when the relative error is smaller or equal than 2 %. As a result, meshes with 186,186 elements for pressurization, 187,302 elements for depressurization at center outlet and 194,996 elements for depressurization at top outlet are chosen. Examples of final optimal meshes for pressurization and depressurization models are shown in Fig. 2.
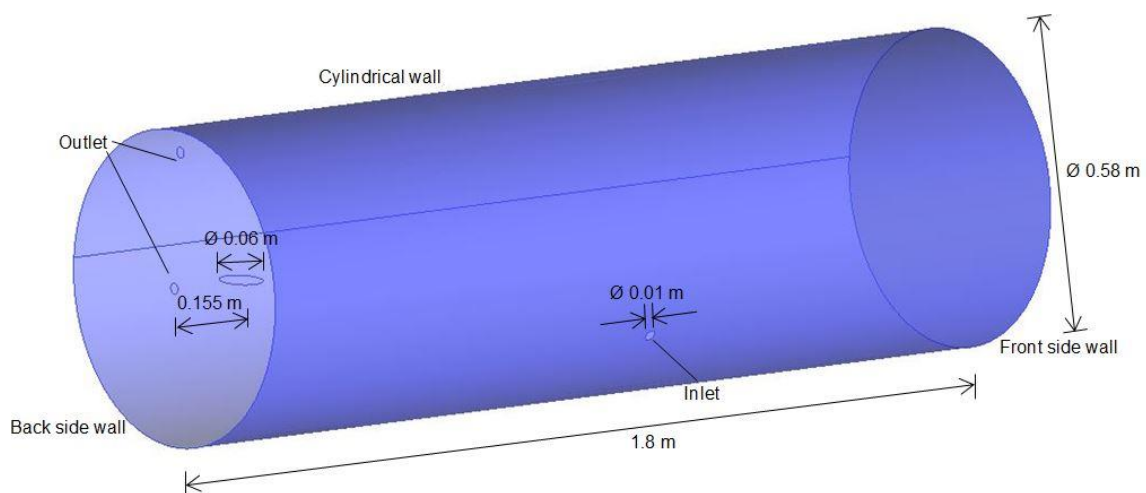

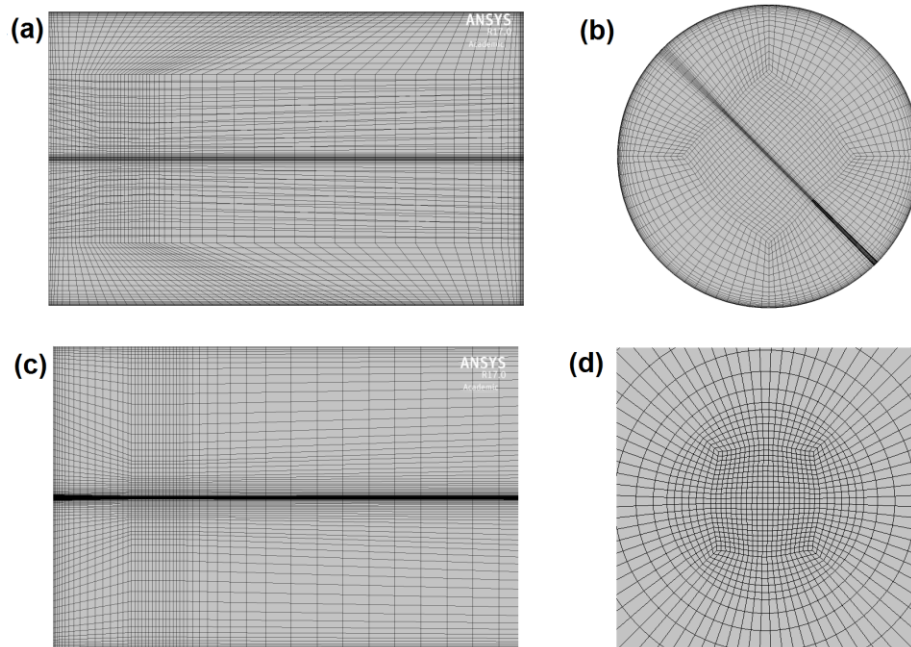Fig. 1: Model geometry developed with ANSYS ICEM with domain boundaries

Fig. 2: (a) Mesh at half of the horizontal plane and (b) mesh at vertical plane in the middle of the reactor for pressurization purpose. (c) Mesh at half of the horizontal plane and (d) mesh at vertical plane for depressurization purpose at center outlet.

The flow field characterization results from an unsteady flow of a slightly compressible single phase fluid in the vessel. The inlet velocity ranges from 0.36 m/s to 0.96 m/s for pressurization and from 1.4 m/s to 3.5 m/s for depressurization. The kinematic viscosity of the fluid (water at 13 °C) is $1.2005 \times 10^{-6} \, \text{m}^2 \, \text{s}^{-1}$. According to the Reynolds number inside the vessel, a simplified numerical set-up of laminar model is developed.

The material properties of water at 13 °C are set as following: density of 999.4 kg m^{-3}, specific heat capacity of 4188.1 J kg^{-1}K^{-1}, dynamic viscosity of 1.2005×10^{-3} kg m^{-1} s^{-1}, thermal conductivity of 0.5855 W m^{-1} K^{-1} and thermal expansivity of 1.258×10^{-4} K^{-1}. Density of water which is injected into the reactor at a constant temperature of 4°C is given based on the experimental data of pressure changing with time. The 2 back and front side walls as well as the cylindrical wall are considered as adiabatic with no slip boundary condition.

The mass flow rate entering or leaving the Simulator depends on the density variation of water as a function of pressure. During the pressurization phase, pressure is increased from 9.912 to 99.768 bar in 86 s. At 86 s, a wall is placed in the inlet boundary to prevent more water from flowing into the reactor. During the depressurization phase, pressure decreases from 99.252 bar to around 11.172 bar in 16 s. After that, a wall will be placed at the outlet boundary to prevent fluid from flowing out of the reactor. In both cases, the change of pressure with time is in good agreement with the experimental trials as presented in (Agudo et al., 2015).

Based on the given flow conditions, the following equations are to be solved: continuity equation, Navier-Stokes equations and the enthalpy equation. As a coupled solver, CFX solve all three momentum equations and the pressure equation in the same matrix. The solution is advanced in time by means of a second order backward Euler-method. According to our temporal discretization study, optimal time step size of 0.001 s is chosen. All the solutions are considered to be fully converged when the residual cut-off value (RMS) of velocity, pressure and mass conservation is below 10^{-4}.

Simulation Results and Discussion

The flow velocity profile in the region of interest, i.e. where the MH is located inside the high pressure vessel during pressurization and depressurization phases, following a change in pressure is characterized. Simulation outcome is validated with experimental results from PIV with regards to three aspects: velocity vector, flow tendency and magnitude of maximum velocity. Characterization of velocity profile is essential to ensure that stability of MH samples as well as the dissociation of MH are not affected by non-desired currents arising from pressure change.

Fig. 3 depicts the simulation results of instantaneous velocity vector field from the top view during and after a sudden increase of pressure to 100 bar in around 85 seconds. After 50 seconds during pressurization (Fig. 3 (a)), the maximum velocity magnitude reaches 0.972 mm/s. The flow velocity at this horizontal observation plane during the process of water injection remains very low, showing no distinctive fluid flow. This agrees well to the experimental observation where the instantaneous velocity barely changes and is only slightly perturbed by convective currents. Immediately after the desired pressure of 100 bar is achieved and water stops being injected into the vessel, two effects can be seen: i. the flow velocity starts increasing and ii. the velocity vector starts changing direction. At 30 second after pressurization, the maximum velocity magnitude reaches 3.69 mm/s. The velocity flow direction can be seen changing its direction constantly in Fig. 3 (b) to (d) from 30 second and this persists until 4 minutes after water injection stops.
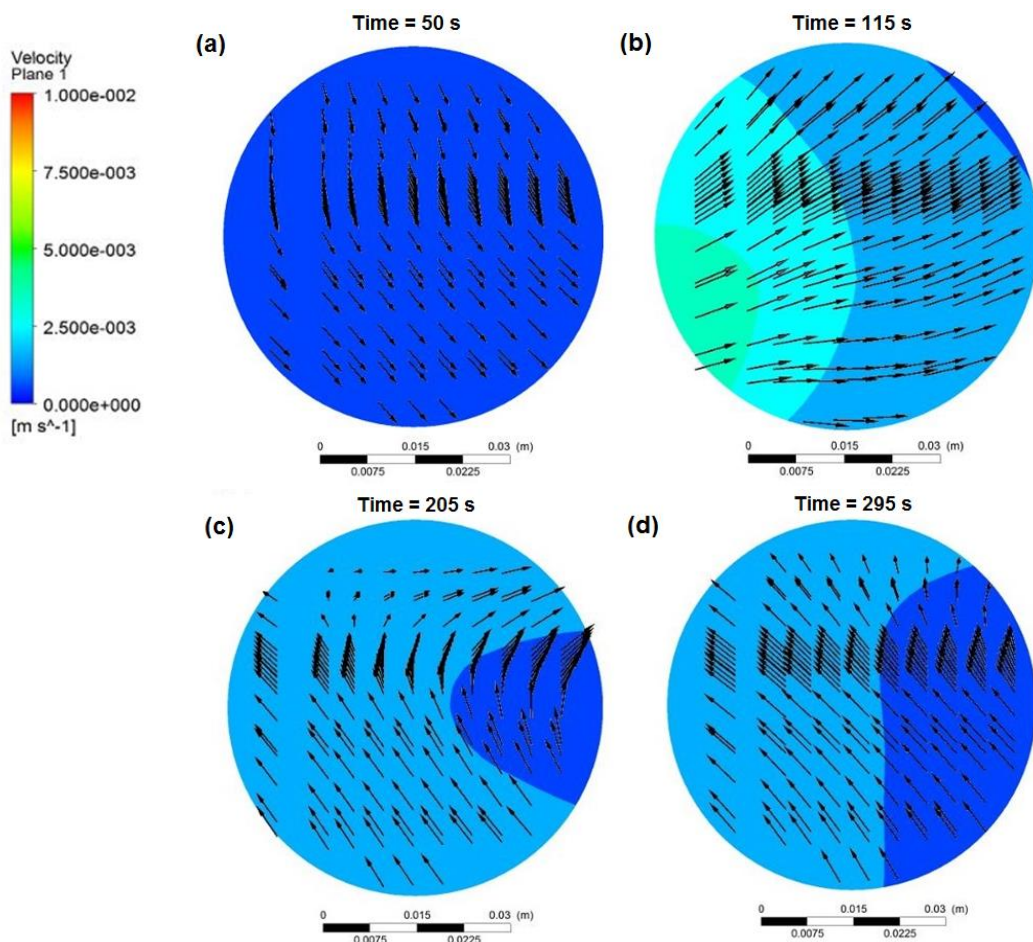

Fig. 3: Vector map of velocity flow field on the horizontal plane (a) at 50 second during pressurization, (b) 30 seconds after final pressure is achieved, (c) 2 minutes after final pressure is achieved and (d) about 4 minutes after final pressure is achieved.

This phenomenon complies with the experimental measurements where a flow recirculation is observed in the horizontal observation plane. Experimental results show a maximum instantaneous velocity of 5 mm/s during the recirculation period while a maximum value of 3.9 mm/s is obtained from the simulation at 50 second after pressurization. About 5 minutes after pressurization, the flow rate decreases to 1.5 mm/s in experiment. This agrees well with the simulation results of a value of 1.4 mm/s at 4 minutes after pressurization stops.

Fig. 4 (a) and (b) show how the velocity flow field in the whole horizontal plane in the vessel develops during an increase of pressure from 36 bar to 95 bar. At 95 bar, fluid flow near the wall is disrupted and higher velocity magnitudes can be observed. This effect is seen to be the cause of the recirculation phenomenon observed in simulation and during experimental PIV measurements. At 30 second after pressurization stops (Fig. 4 (c)), fluid flows from the wall into the observation area which causes an increase in velocity as well as changes in velocity flow direction and in turn flow recirculation. After maximum flow velocity is achieved, the fluid flow is dispersed into other direction, resulting in lower velocity magnitude at the observation area as shown in Fig. 4 (d). The circulation process only starts after the water injection stops, which implies a strong influence from the diffusive momentum flow.

Further simulations for a depressurization process at the center outlet from 100 bar to 10 bar in 17 s at a constant temperature of 13 °C are performed. During depressurization, water is directed to the center hole at the back side wall of the reactor. At 0.2 second, a maximum velocity magnitude of 3.33 mm/s is detected on the horizontal observation plane while experimental result shows a value 5.99 ± 0.69 mm/s. After reaching the maximum velocity, flow velocity keeps decreasing while the fluid continuously flows towards the outlet direction. Immediately after depressurizations stops, a maximum instantaneous velocity of 1.19 ± 0.10 mm/s is measured by PIV in experiments. In simulation, a maximum value of 0.99 m/s is obtained at 17.1 second following an abrupt closing of the valve. At this time, the flow is directed to all directions, showing an agreement with the experimental observation.
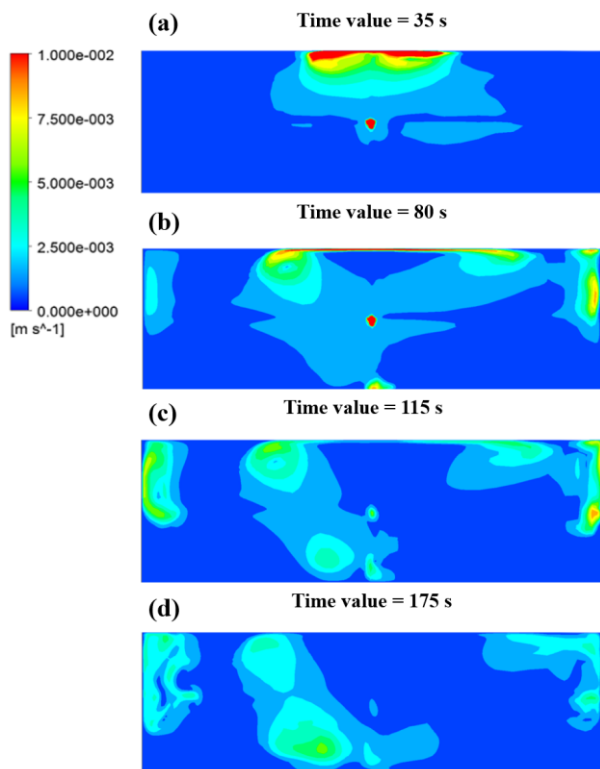

Fig. 4: Velocity contour map at the horizontal plane of the vessel (a) at 36 bar, (b) at 95 bar, (c) at 30 second after pressurization stops and (d) at 90 second after pressurization stops.

During depressurization at the top outlet from 100 bar to 10 bar in 17 s at constant temperature of 13 °C, water is directed to the outlet at the back side wall of the reactor. Fig. 5 depicts the comparison of simulation and experimental results during the process. At 0.2 second, a maximum velocity magnitude of 1.09 mm/s is detected on the plane of interest according to the simulation result in Fig. 5 (a) which lies within the PIV measurement results of 1.05 ± 0.18 mm/s. After reaching the maximum velocity, flow velocity keeps decreasing. During a decrease in flow velocity, the velocity flow direction changes. Instead of flowing in one horizontal direction, it is directed to all directions outward as seen in Fig. 5 (b). This aspect shows a resemblance with the experimental illustrations. Immediately after the valve is closed, a maximum instantaneous velocity of 0.9 ± 0.07 mm/s is measured by PIV. Simulation result in Fig. 5 (c) gives a value of 0.97 mm/s which again lies well within the PIV measurement range. The fluid continues to flow in all directions right after depressurization process stops and this conforms to the experimental observation.
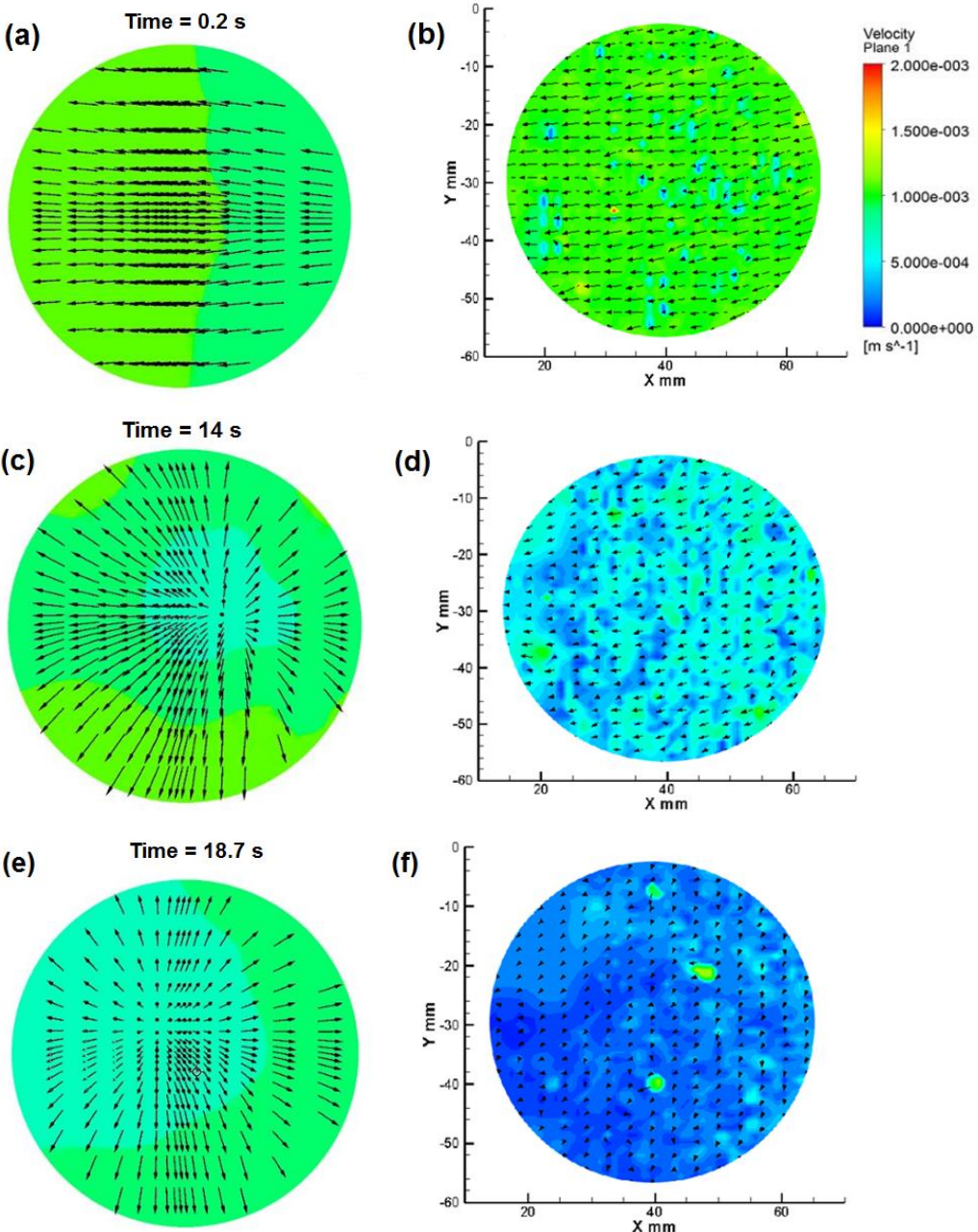

Fig. 5: Vector map of velocity flow field at horizontal plane (a) – (b) at 0.2 second during depressurization at top outlet, (c) – (d) at 14 second during depressurization at top outlet and (e) – (f) after closing of valve following simulation (left) and PIV measurements (right).

Summary and conclusion

The velocity flow field change due to fluctuation of pressure on the deep sea simulator is thoroughly studied here. The numerical results during pressurization and depressurization at center, and at the top outlet of the vessel are in very good agreement with previous PIV results. In pressurization experiments, convection current could be expected due to the temperature gradient between the wall and the bulk of water. However, flow velocities in the horizontal observation area remain stationary during fluid injection, proving that thermal effect is eliminated here. This fact has been experimentally observed by measuring same temperature values at different points of the reactor (see Agudo et al., 2015). Also, a constant temperature had been set up in simulation. A flow recirculation with a maximum velocity of 3.9 mm/s at the horizontal plane of interest, which is reduced to 1.4 mm/s at 4 minutes after achieving the maximum pressure, occurs in simulation as well as in experiment and is seen to develop because of diffusive momentum change. During depressurization, numerical results show that the maximum velocity at the observation plane during water removal from center outlet (3.33 mm/s) is much higher than from the top outlet (1.9 mm/s). However, after a sudden closing of valve, a flow velocity approaching zero is observed in both cases. Strong evidence of stationary velocity profile inside the vessel just a few seconds after the sudden decrease in pressure can be seen. This conclusion enables a correct quantification of gas release during GH dissociation through indirect measurement of velocity flow profile fluctuation in the vessel in further experiments. As the velocity remains stationary inside the vessel, any changes in velocity field will not be regarded as an effect from non-desired currents but is identified to be solely the release of gas produced from solid hydrates. The good agreement between the simulation results and experimental observations provides us a key for better understanding of GH dissociation mechanism.

References

Agudo J.R., Park, J., Rauh C., Wierschem A., Delgado A. (2015) Methane hydrate extraction under high pressure conditions (PIV measurements), Fachtagung „Lasermethoden in der Strömungsmesstechnik" Dresden

Archer D. (2007) Methane hydrate stability and anthropogenic climate change, Biogeosciences Discussions, European Geosciences Union, 4 (2), 993-1057.

Bachu S. (2000) Sequestration of CO2 in geological media: criteria and approach for site selection in response to climate change: Energy Conversion & Management, 41, 953-970

Haugan P.M., Drange H. (1992) Sequestration of CO_2 in the deep ocean by shallow injection, Nature, 357, 318-320

Janicki G., Schlüter S., Hennig T., Deerberg G. (2014) Simulation of subsea gas hydrate exploitation, Energy Procedia, 59, 82 – 89

Kajishima T., Saito T., Nagaosa R., Kosugi S. (1997) GLAD: A gas-lift method for CO2 disposal into the ocean. Energy 22, 257–262

Kelkar V., Mishra R., Mohan N., Joseph E. (2014) IOSR Journal Of Environmental Science, Toxicology And Food Technology (IOSR-JESTFT), 8, 85-88

Kim Y.G., Lee S.M., Jin Y.K., Branov B., Obzhirov A., Salomatin A., Shoji H. (2013) The stability of gas hydrate field in the northeastern continental slope of Sakhalin Island, Sea of Okhotsk, as inferred from analysis of heat flow data and its implication for slope failures, Mar. Petrol. Geol., 45, pp. 198-207

Kvenvolden K.A. (1993) Gas hydrates – Geological perspective and global change. Reviews of Geophysics, 31, 173-187

McGrail B.P., Schaef H.T., White M.D., Zhu T., Kulkami A.S., Hunter R.B., Patil S.L., Owen A.T., Martin P.F. (2007) Using carbon dioxide to enhance recovery of methane from gashydrate reservoirs: Final Summary Report, Pacific Northwest National Laboratory, United States Department of Energy

NPARC Alliance CFD Verification and Validation Website: http://www.grc.nasa.gov/WWW/wind/valid/tutorial/spatconv.html

Sloan E.D., Koh C.A. (2008) Clathrate Hydrates of Natural Gases, Third Edition, CRC Press, Taylor & Francis Group

Tishchenko P., Hensen C., Wallmann K., Wong C. S. (2005) Calculation of the stability and solubility of methane hydrate in seawater, Chemical Geology, 219, 37-52

Zhang Z., Wang Y., Gao L., Zhang Y., Liu C. (2012) Marine Gas Hydrates: Future Energy or Environmental Killer?, Energy Procedia, 16, 933 – 938